

# PROPELLER AEROACOUSTIC MODELS IN VARIABLE-FIDELITY DESIGN OPTIMIZATION

Witold Klimczyk<sup>1</sup> & Adam Sieradzki<sup>2</sup>

<sup>1</sup>Department of Aerodynamics, Lukaszewicz Research Network — Institute of Aviation, al. Krakowska 110/114, 02-256 Warsaw, Poland, email: Witold.Klimczyk@ilot.lukasiewicz.gov.pl

<sup>2</sup>Department of Aerodynamics, Lukaszewicz Research Network — Institute of Aviation, al. Krakowska 110/114, 02-256 Warsaw, Poland, email: Adam.Sieradzki@ilot.lukasiewicz.gov.pl

## Abstract

Variable-fidelity modeling-based (VFM) optimization frameworks are commonly used to reduce the cost of the optimization processes. Where the optimization based on cheap, low-fidelity code does not lead to high-fidelity optimum, addition of limited calls to the expensive high-fidelity code, allows to exploit low-fidelity trends in obtaining high-fidelity optimum. The potential of variable-fidelity modeling is especially prominent in the field of Computational Fluid Dynamics (CFD)-based optimization, where the cost of high-fidelity simulations is typically very high. Whereas the purely aerodynamic optimization using variable-fidelity models is well documented, the approach is rarely applied to propeller aeroacoustic optimization.

In the current work, selected propeller aeroacoustic models were analyzed in terms of their usefulness in the design of low-Reynolds-number propeller blade. The analyzed methods include: low-fidelity Blade Element Theory (BET)-based model, and high-fidelity blade-resolved CFD model for aerodynamics and tonal noise. Additionally, the semi-empirical broadband noise models were used to complete the noise spectrum. Firstly, the models were compared and validated against the experimental benchmark from the literature. Hence, the analysis of trends and correlations between models of different fidelity was performed. It was found, that both BET-based and CFD-based models give similar changes to force and noise predictions, after chord or twist modification to the baseline geometry is applied. The correlations calculated for a sample of design points with different geometries were established. Both aerodynamics and noise predictions are highly correlated — with  $r_s$  ranging from 0.86 to 0.95, depending on the data set.

Finally, the discussion on the VF optimization process to be built with the presented methods summarizes its advantages and limitations.

**Keywords:** propeller aeroacoustics, propeller design, CAA, noise reduction, variable-fidelity optimization

## 1. Introduction

Variable-fidelity (VF) design optimization (also known as, among others: *multi-fidelity* or *variable-complexity*), is considered as one of the most efficient global optimization frameworks. It is especially useful in design problems, which involve expensive (time or CPU-consuming) simulations, such as the aerodynamics-based problems. The variable-fidelity modeling (VFM)-based optimization framework makes use of models, which provide data of different fidelity and at different cost. Typically, high-fidelity (HF) model is defined as a model with sufficient fidelity for particular task. On the other hand, low-fidelity (LF) model provides data with some inaccuracy — the source of which may be different. The single and multi-fidelity based optimization processes are schematically shown in Figure 1.

The typical implementation is achieved by utilization of a surrogate model, with the dominance of kriging-based methods (co-kriging, hierarchical kriging). In this work, the use of co-kriging [1] approach to VF surrogate modeling is assumed — its requirements and features were assumed where it was necessary. The typical VFM-based optimization process can be summarized in the following steps. Firstly, the cheap LF model can be used extensively to cover large sample of design points and provide trends of the objective function. However, the lack of fidelity limits the confidence of obtained result. The HF model is then ran on sparse data sample, with the goal of establishing the difference

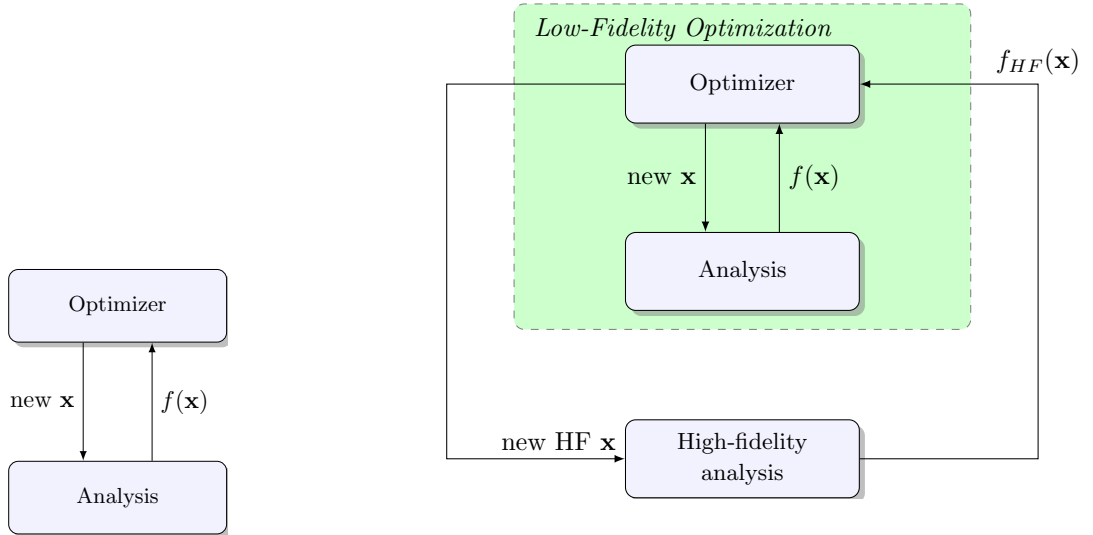


Figure 1 – Single-fidelity (left) and variable-fidelity (right) optimization data flow.

between both models. The VFM (such as co-kriging) is calculated from these two data sets. It allows to predict the unknown function value at any point within the search space. The resulting VF model provides highly accurate predictions for smooth functions, as well as it is suited for optimization guidance, by means of error prediction-based exploration and exploitation [1], [2]. The ultimate goal of VF optimization is to achieve the result identical to pure HF-model based optimization, at a significantly reduced cost.

Table 1 presents literature examples of VF optimization in aerodynamics-based design. An important feature of VFM frameworks is the freedom in selection of LF model, which is expected to provide the most effective speedup to defined HF model. The nature of fidelity trade-off in LF model can be attributed to: physics (simplified model, lower dimensionality etc.), discretization (coarse/fine mesh, convergence criteria). Consequently, the selection of LF/HF models is largely dependent upon the process designer experience and intuition. The authors did not come across the use of VFM frameworks in the aeroacoustic propeller design. The need for a study, which allows to make reliable choices in preparation of VF optimization framework was therefore identified.

Table 1 – Selection of multi-fidelity optimization setup found in literature.

work	low-fidelity	high-fidelity	variables	framework
[1]	empirical	VSAero	11	co-kriging
[3]	vortex lattice	RANS		multidisciplinary
[4]	RANS (coarse)	RANS (fine)	8-12	co-kriging
[5]	Euler (0.25m cells)	Euler (3-5m cells)	17	multidisciplinary
[6]	full potential boundary layer	RANS	36	co-kriging
[7]	single-point	multi-point	2-30	co-kriging, multi-point
[8]	Euler	RANS SA	1,3	hierarchical kriging

The main decisions to be made when designing the optimization procedure include the definitions of high and low fidelity models as well as the number of high and low-fidelity sample points. The general rules for construction of an efficient multi-fidelity model require highly correlated models and dense low-fidelity sampling [9]. These, however, are case-specific, and additional study should be made to confirm the expectations.

In this work a comprehensive study aimed to build the variable-fidelity framework for aeroacoustic propeller blade design was performed. Variable fidelity models for analysis of low-Reynolds number propeller in hover were examined.

This work is structured as follows: in section 2, the aerodynamic and aeroacoustic models are described. In section 3, the models are compared for the benchmark propeller, hence, the basic trends

are compared. In section 4, the comparison of models, with emphasis on their potential in VF optimization framework is presented. The correlations between data collected using VF models are established. The conclusions and further work are summarized in section 5.

## 2. Computational aeroacoustic models

Analyses performed in the current work were focused on the aeroacoustic performance of low-Reynolds number propellers. The air sea-level conditions were used for fluid properties. The rotational speed was  $5000\text{ rpm}$  ( $\Omega = 523.6\text{ rad/s}$ ). The thrust ( $C_T$ ) and torque ( $C_Q$ ) coefficients used throughout the paper are defined as:

$$C_T = \frac{T}{\rho_\infty \pi \Omega^2 R^4}, \quad (1)$$

$$C_Q = \frac{Q}{\rho_\infty \pi \Omega^2 R^5}, \quad (2)$$

where  $\rho_\infty$  is the freestream density and  $R = 0.15\text{ m}$  is the propeller tip radius. The noise levels are defined by overall sound pressure level (*OASPL*):

$$OASPL = 20 \log_{10} \frac{p_{rms}}{p_0}, \quad (3)$$

where  $p_{rms}$  is the root-mean-square sound pressure and  $p_0 = 2 \times 10^{-5}\text{ Pa}$  is the reference pressure. The selection of aerodynamic and aeroacoustic models is non-trivial task, due to the computational cost versus model fidelity trade-off. Propeller/rotor noise modeling was investigated by numerous researchers, with significant progress made in 1970s and 1980s. A number of low-fidelity methods for tonal noise calculation were developed [10]. The accuracy of tonal noise prediction is inherently coupled with the accuracy of aerodynamic forces on the blade, which influence the loading part of the noise.

Recent approaches to model the propeller noise rely on the turbulence resolving CFD, such as the Large Eddy Simulation (LES)-based models (including hybrid RANS-LES) or the Lattice Boltzmann Method (LBM) [11]. They allow to calculate not only tonal, but also broadband noise basing on the CFD model.

In the current work, two models were selected for further analysis and comparison: high and low fidelity models are described in this section.

### 2.1 High-fidelity model

The high-fidelity (HF) model used in the current work was based on the solution of finite-volume CFD model using commercial code *Ansys Fluent 21.1*. The turbulent, two-equations  $k - \omega$  SST [12] steady RANS model was solved for single blade in periodic, multiple reference frame (MRF), rotating domain setup, as shown in Figure 2. The incompressible, coupled pressure-based solver was used due to local Mach not exceeding 0.3 (tip speed was around Mach 0.23). The domain extended 40 radii in directions normal to rotating plane and 24 radii along the blade radius. The hover was modeled by setting boundary conditions on the domain boundaries to low-turbulence pressure-outlets.

Second order and second-order upwind schemes were selected for pressure and convection terms of governing and turbulence model equations to reduce the numerical dissipation. 3000 iterations were performed for each case, to ensure convergence. This was sufficient for the continuity residuals to drop at least 8 orders of magnitude. Turbulence intensity upstream of the blade was additionally monitored to ensure the solution convergence.

A two-steps mesh study was performed to establish optimum mesh sizing for automated unstructured polyhedral meshing procedure. Firstly, the surface mesh was refined to find the coarsest grid settings with sufficient detail to give mesh-independent solution. The minimum cell size (0.025mm) and curvature angle ( $9^\circ$ ) were defined as global mesh settings. Hence, the volume mesh study, including both near-wall region (prism layers) and volume mesh refinement regions was performed. The study showed that 25 prism layers covered the whole boundary layer, with  $y^+$  not exceeding 5. The volume mesh refinement was necessary in the region surrounding the blade, particularly in the region of tip-vortex of preceding blade and in the slipstream. The mesh study summary for test blade

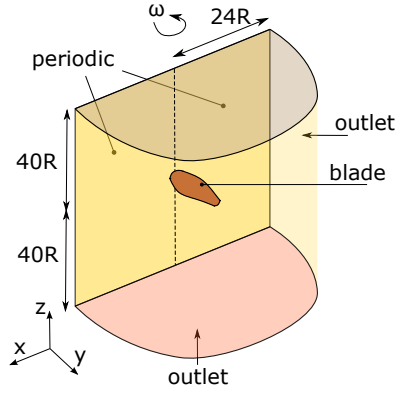


Figure 2 – Schematic view of the computational domain. Two blades-propeller implies 180° rotational periodic boundaries. The inlets on the top and side boundaries of the domain are pressure-outlets for hover.

geometry is presented in Figure 3. The surface mesh with around 115 thousand elements (left plot) was deemed sufficient for current work, as for both  $C_T$  and  $C_Q$  clear convergence trend is observed. The volume mesh refinement affecting the sizing on periodic boundaries as well as the refinement of surface mesh near the leading and trailing edges of propeller blade are presented on the right of Figure 3.

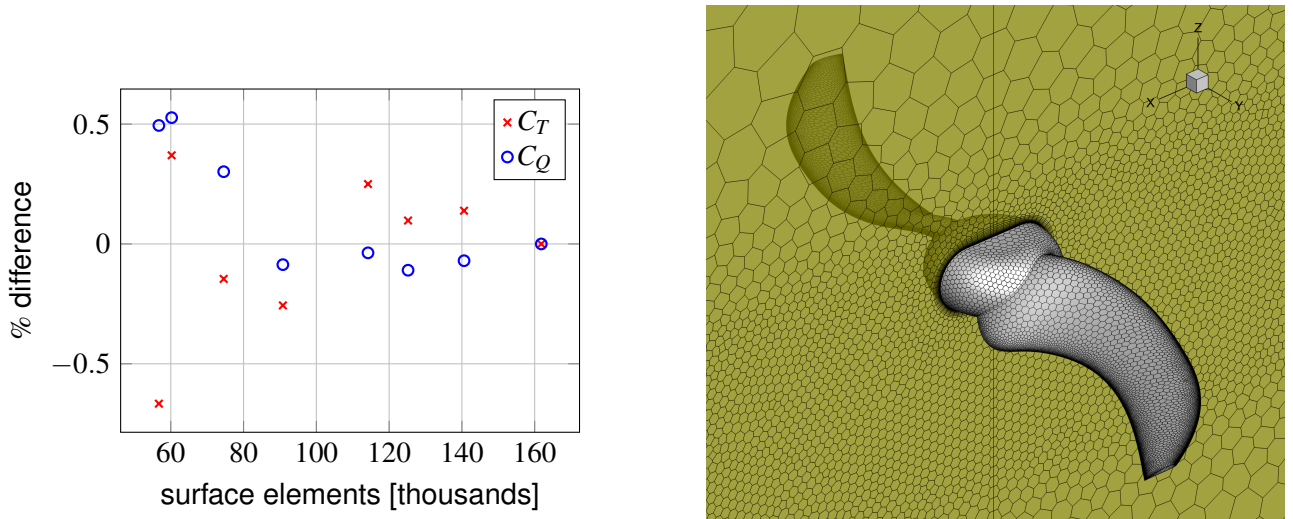


Figure 3 – Surface mesh study summary (left) and mesh sizing in different regions (right). Axial duplication was shown to give the overview on the modeled geometry.

## 2.2 Tonal noise

The tonal noise was calculated using Farassat 1A formulation [13] of Ffowcs-Williams and Hawkings (FWH) acoustic analogy [14] based on the solution of CFD model. The acoustic pressure  $p'$  is defined as:

$$p'(\vec{x}, t) = p'_T(\vec{x}, t) + p'_L(\vec{x}, t) \quad (4)$$

$$4\pi p'_T(\vec{x}, t) = \int \left[ \frac{\rho_0 (\dot{U}_n + U_n)}{r(1-M_r)^2} \right] dS + \int \left[ \frac{\rho_0 U_n \{ r\dot{M}_r + a_0 (M_r - M^2) \}}{r^2 (1-M_r)^3} \right] dS, \quad (5)$$

$$4\pi p'_L(\vec{x}, t) = \frac{1}{a_0} \int \left[ \frac{\dot{L}_r}{r(1-M_r)^2} \right] dS + \int \left[ \frac{L_r - L_M}{r^2 (1-M_r)^2} \right] dS + \frac{1}{a_0} \int \left[ \frac{L_r \{ r\dot{M}_r + a_0 (M_r - M^2) \}}{r^2 (1-M_r)^3} \right] dS, \quad (6)$$

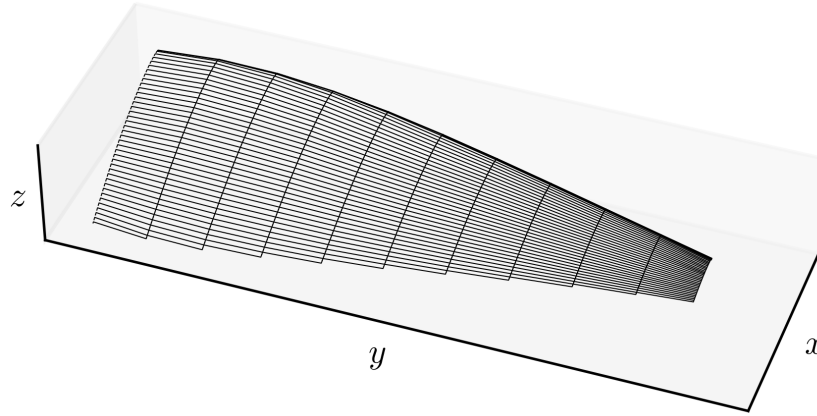


Figure 4 – LF model: blade's top surface representation with panels. Three-dimensional features of blade geometry are accounted for in acoustic calculations.

where:

$$U_i = v_i + \frac{\rho}{\rho_0} (u_i - v_i), \quad (7)$$

$$L_i = P_{ij} \hat{n}_j + \rho u_i (u_n - v_n). \quad (8)$$

Here,  $u$  is the fluid velocity,  $v$  is the surface velocity,  $P_{ij}$  is the compressive stress tensor, subscript  $i$  denotes coordinate direction and  $n$  — direction normal to the surface. The integrals are evaluated over the integration surface (typically denoted by  $f = 0$ ) — which is the impermeable propeller surface and in the emission time. Vector  $\vec{x}$  defines observer's position relative to the noise source.

The relative cost of tonal noise calculations based on steady CFD model is low as the same CFD solution is used to construct acoustic pressure signal. The acoustic pressure signal was recorded for 50 revolutions and 30 times per revolution. The resulting sampling gives the spectral resolution of  $6.7Hz$  and covers BPF and its harmonics up to  $f = 6000Hz$ .

### 2.3 Low-fidelity model

The low-fidelity model used in the current work was based on the aerodynamic blade-element/vortex method code QPROP [15]. The robustness of QPROP is especially important in case of hovering rotors. The aerodynamic solution provides force coefficients as well as local flow field parameters: including local angle of attack and velocity. The panel geometry was generated on defined number of spanwise and chordwise stations. The three-dimensional features of geometry are represented, as is presented in Figure 4. Hence, the chordwise pressure distribution on each station along the span was found using XFOIL [16] and the pressure over whole blade was interpolated to the panel's centers. The acoustic pressure was calculated using the non-permeable Farassat 1A [13] with linear interpolation-based source-time dominant retarded-time approach [13].

### 2.4 Broadband noise

In the case of smaller propellers, typical for unmanned aerial vehicles or urban air mobility vehicles, broadband noise can have a significant impact on the overall noise level [17]. Therefore, in the current work, semi-empirical models were used to roughly estimate the contribution of broadband noise. The relations developed by Brooks, Pope and Marcolini [18] were used to predict the turbulent boundary layer-trailing edge noise, as well as the trailing edge bluntness noise. The turbulent inflow noise was calculated using a simplified linear version of the Guidati method [19]. In this study, the implementation of above methods available in the NAFNoise software [20] was used. NAFNoise was developed to predict the noise generated by an isolated airfoil (wing section). XFOIL routines [16] were used to enable the calculation of boundary layer properties for any airfoil shape. The input data to the analysis included parameters such as flow velocity and angle of attack, which in this study were determined on the basis of the LF model for several blade sections. Then, the noise contribution of each section was calculated. In order to obtain a spectrum of total propeller noise for a given observer

location, all the sources were added logarithmically taking into account the noise directivity and the Doppler effect resulting from blade rotation. The procedure was repeated for several different angular positions of the blades, obtaining changes in propeller noise over time. In the last step, the average noise spectrum was determined.

### 3. Analysis of variable-fidelity models

The analysis of results obtained from models described in previous section was based on the benchmark described in the literature [11]. The geometry of a benchmark propeller was based on the stacking of *NACA4412* airfoil along the radius with chords and twist distributions shown in Figure 5. The difference in geometry compared to the original benchmark is the stacking line — in the current work airfoils were stacked along spanwise *y*-axis with reference position at  $x/c = 0.4$ , i.e. at 40% chord. The noise was calculated at observer positions located at a distance of  $1.2m$  ( $8R$ ) from the rotation axis. Three positions: in-plane ( $z = 0$ ), downstream ( $z = -0.9m$ ) and upstream ( $z = 0.9m$ ) were selected for microphones: mic 0, mic 1 and mic 2, respectively.

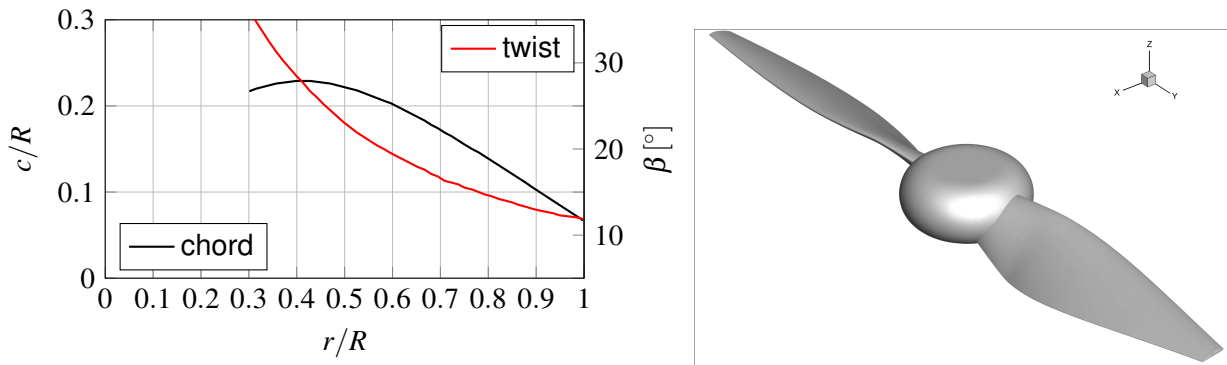


Figure 5 – Benchmark geometry - chord and twist distributions (left) and CAD geometry used in CFD (right).

#### 3.1 Aerodynamics and noise prediction

The summary of thrust and torque obtained for benchmark propeller is presented in Table 2. The differences are very small.

Table 2 – Comparison of thrust and torque coefficients obtained for baseline propeller using HF and LF. Experimental data [11] added for reference.

model	$C_T$	$C_Q$
HF	0.0156	0.00222
LF	0.0152	0.00221
Exp	0.0149	0.00194

The differences in forces prediction are a result of limitations of LF aerodynamic model as well as inaccuracies of HF model. In the context of multi-fidelity modeling, the auto-regressive form of the VF framework is assumed, i.e. inaccuracies lie wholly in the LF model. Consequently, only LF limitations in relation to HF model are discussed.

Firstly, the limitation of QPROP, which models airfoil data only in their linear lift regime. If the local angle of attack exceeds the maximum angle of attack of the linear regime (or is lower than minimum), the local lift coefficient  $C_L$  value is clipped to maximum (or minimum) value. Consequently,  $C_L$  values can be inaccurate, either too large or too low, depending on the case. The drag coefficient  $C_D$  on the other hand, is highly penalized if local angle of attack falls outside the linear  $C_L$  regime. This is summarized in Figure 6 which shows the radial distribution of lift and drag on the blade along with the local effective angle of attack  $\alpha_{eff}$ . It can be observed that almost the whole blade operates at  $\alpha_{eff}$  exceeding the maximum of linear  $C_L$  range of local airfoil.  $C_L$  values are clipped to just above unity (the

value changes with local Reynolds number), while  $C_D$  increases up to 0.25 near hub. The effective angle of attack is very high, especially near the hub, which is expected for a propeller designed for higher advance ratio. The limitation of QPROP is especially important for low-Reynolds number propellers, with the same airfoils operating at higher Reynolds numbers having their linear  $C_L$  regime extended.

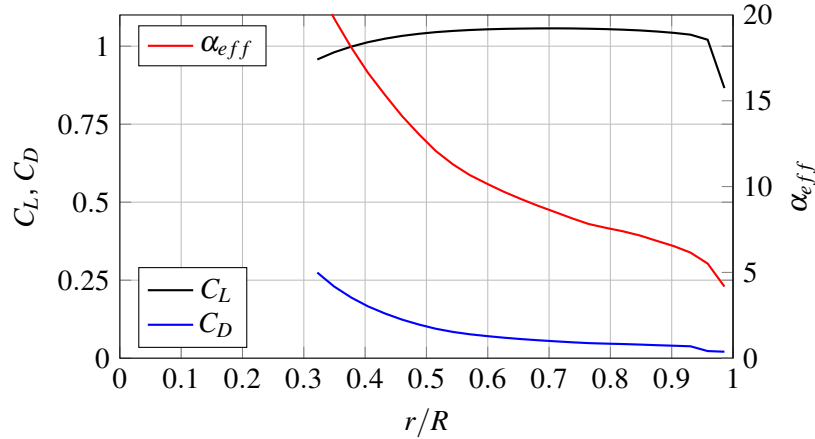


Figure 6 – Benchmark geometry results obtained from LF model.

Secondly, the LF model has limitations in modeling the effect of tip and blade-vortex interaction, particularly important in hover. The HF model visualization presented in Figure 7 shows the significance of blade-vortex interactions on the aerodynamics of the propeller in hover. The  $q$ -criterion contour map shows the location of the center of tip-vortices — the red color indicates the slipstream, i.e. the first vortex is centered around  $0.2R$  below the blade, while the second is around  $0.5R$  downstream. The normalized turbulent kinetic energy (TKE) plot indicates the region of highly turbulent flow. It should be noted, that the volume mesh refinement region was defined down to around  $z/R = -0.8$  — the model around and below this region has limited quality.

For both LF and HF models, the tonal noise calculation is based on the impermeable FWH. The acoustic pressures found with LF and HF models at mic 0 and mic 1 are presented in Figure 8. The signals have similar shapes, their peaks and zeros are located on the same time-axis positions. The difference in the amplitude of oscillations is relatively large for mic 0 and results in a significant difference in OASPL. For mic 1, the amplitude is very similar, with the small shift in HF signal.

The total noise emitted by a rotor is found by adding the tonal and broadband constituents. In Figure 9, the SPL in 1/3 octave bands is presented. The noise spectra obtained with computational approach used in the current work are close to the experimental results [11] added for reference. Importantly, the relatively large difference in SPL around  $f = 1000Hz$  results from motor noise.

### 3.2 Local trends analysis

The local trends analysis was performed to assess the basic influence of design parameters on the models output. This study was performed for a baseline propeller built with stacking of two airfoils — *mh116* at  $0.2R$  and *mh117* at the tip, linearly interpolated to required radial sections. The effect of varying three parameters on aerodynamics and noise was checked, i.e. chord, twist and sweep. The baseline was defined with the same radial distributions as the benchmark geometry. Hence, the chords were scaled by 0.9 and 1.1, propeller pitch was increased and decreased by  $1^\circ$  and sweep was increased twice. The resulting study consists of baseline and six additional cases. The summary of trends captured using HF and LF models is given in Table 3. It can be observed, that the percentage changes in thrust and SPL are very similar for chord and twist variations. This confirms the usefulness of LF model, especially in the optimization context. The sweep effect, however, has not been captured by LF model. The limitation of aerodynamic LF model (which does not account for sweep) is passed to noise prediction. The propagation of aerodynamic model error to noise prediction is clear. The sweep importance in aeroacoustic blade design should be noticed — HF model predicts

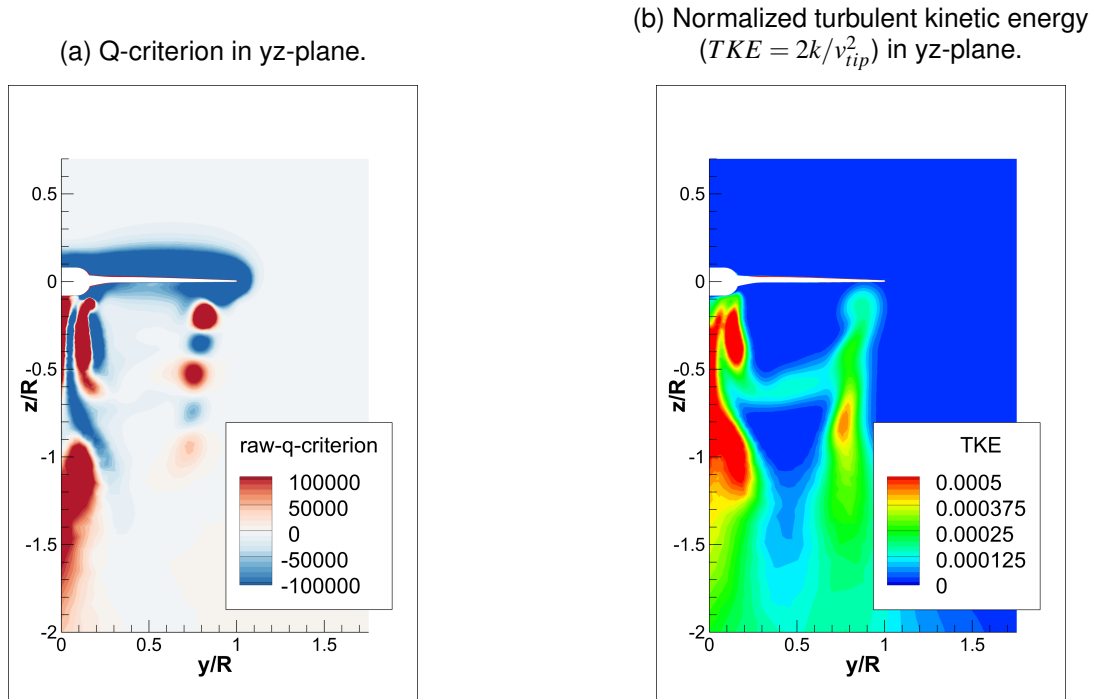


Figure 7 – Contour maps of q-criterion and turbulent kinetic energy of benchmark propeller in hover show the blade-vortices path. The proximity of blade-vortex shed from preceding blade shows the importance of this interaction on aerodynamics.

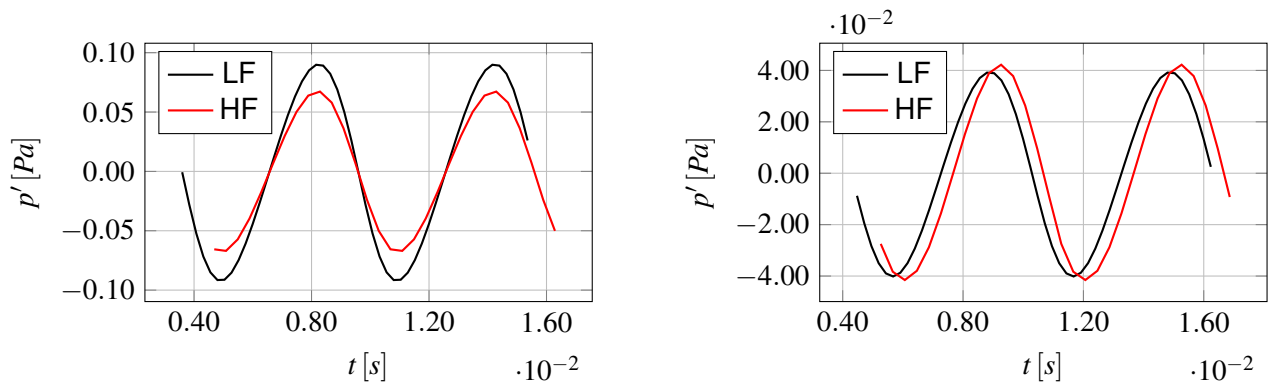


Figure 8 – Acoustic pressure for a single revolution ( $t_{rev} = 0.012$  s) calculated using LF and HF at mics 0 (left) and 1 (right).

even 5.5% increase in thrust for highly swept blade, while the SPL at in-plane observer is slightly decreased.

#### 4. Optimization using variable-fidelity models

The efficient global optimization using models of variable fidelity requires highly correlated models. The typical global optimization is focused on scanning a relatively wide search space and is primarily used to determine the potential global optimum. In the current section, a generic propeller blade geometry definition, which allows to obtain a range of different geometries is described. Hence, the sample of candidates defined using the parametric definition is evaluated using models of different fidelity. The comparison of results obtained with these models is performed, and potential use of these models in VF framework is discussed.

##### 4.1 Generic propeller geometry model

A generic parametric model of a propeller blade geometry was defined as a stacking of airfoils along the span. The variables in the model included:

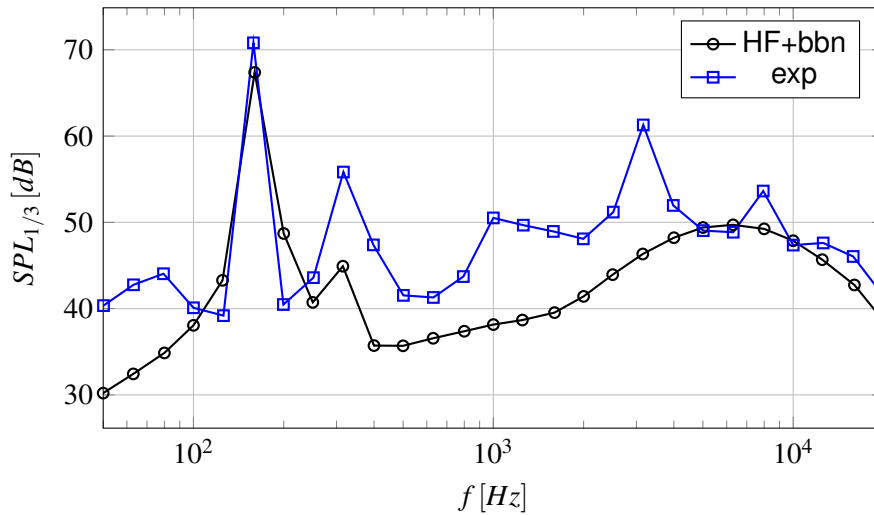


Figure 9 – 1/3 octave band SPL at mic 0, obtained using the HF tonal noise model with added broadband noise contribution. Experimental data [11] added for comparison.

Table 3 – Local trends analysis obtained using LF and HF models, given in percent change of thrust ( $T$ ) and SPL compared to baseline.

	$T_{HF}$	$SPL_{mic0,HF}$	$T_{LF}$	$SPL_{mic0,LF}$
chord $\times 0.9$	-8.3%	-1.8%	-8.1%	-1.5%
chord $\times 1.1$	+5.5%	+1.7%	+4.6%	+1.3%
twist $-1^\circ$	-13.0%	-1.4%	-12.7%	-1.3%
twist $+1^\circ$	+7.1%	+1.6%	+7.5%	+1.2%
sweep1	+1.9%	-0.2%	-	0.0% <sup>1</sup>
sweep2	+5.5%	-0.3%	-	0.0% <sup>1</sup>

- Chord ( $c$ ), twist ( $\beta$ ) and sweep ( $\Lambda$ ) radial distributions. These can be parameterized using selected method. In this work, 5-knots splines were used, which resulted in total of 15 geometric variables and provided a significant design freedom.
- airfoils — defined at required radial positions along the span. In the current work two airfoils were defined — *mh116* at 20% radius and *mh117* at the tip. The geometry was then generated from further interpolated stacking of original airfoils to 25 uniformly distributed radial positions.

The only assumption regarding the blade geometry was the smoothness of radial distributions — such that the resulting geometry was also smooth, and could be lofted through the sections. A sample of 50 points in 15 dimensions was created using latin-hypercube sampling with maximin criterion [21] to achieve random and uniformly sampled search space. Figure 10 presents the sample of blade chord distributions, as defined by five knots fixed in radial direction and varying within specified limits. Similar distributions were created for twist and sweep. The limits were selected to cover a possibly wide search region, while maintaining local angles of attack in the linear lift coefficient regime. Additionally, the target thrust of around  $8N$  for  $\omega = 5000rpm$  was desired.

#### 4.2 Test sample comparison

The sample of 50 cases was analyzed using both LF and HF models. In Figure 11 four propeller geometries randomly selected from the sample are shown to present the variation on geometry within the search space. In Figure 12 the pressure distributions ( $p/(0.5\rho v_{tip}^2)$ ) calculated using HF model are presented.

<sup>1</sup>SPL change is nonzero, but unnoticeable, as the difference is only a result of slightly modified acoustic signal recorded at the microphone.

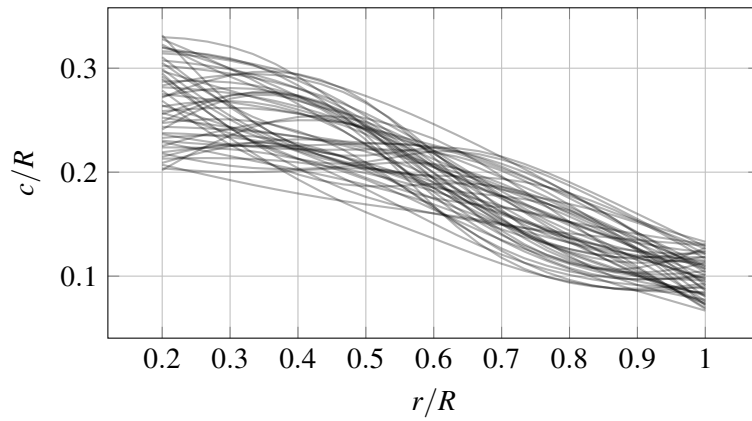


Figure 10 – Chord distributions of a sample of 50 design points.

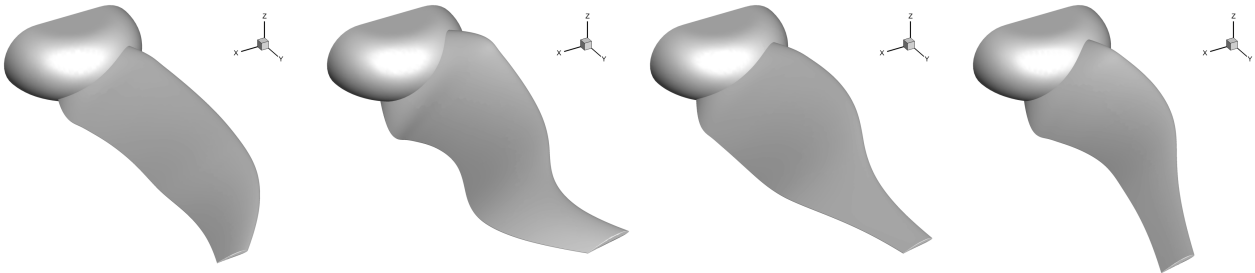


Figure 11 – Four geometries randomly selected from sample.

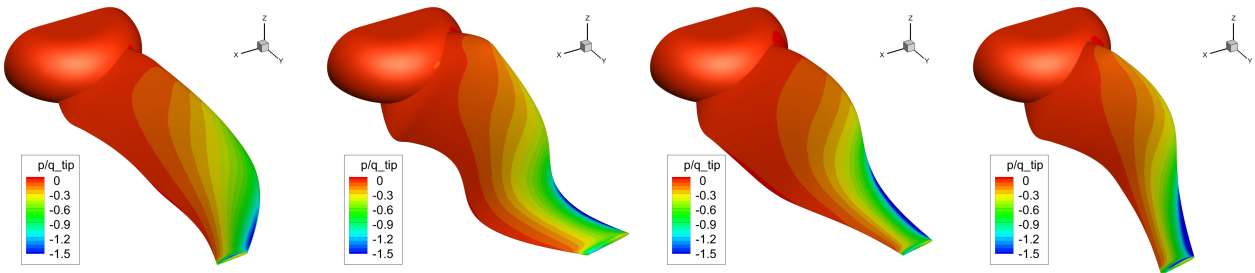


Figure 12 – Pressure distributions on top surface of selected geometries from sample calculated using HF model.

The correlations between LF and HF models were established for test sample and they are summarized in Table 4. Both force and noise correlations are very high, with  $C_T$  and  $C_Q r_s$  of just below 0.9 and OASPL  $r_s$  ranging from 0.88 up to 0.95, depending on the observer location. Figure 13 presents thrust and torque comparison for LF and HF models. Some significant differences in predictions can be observed. These differences are a result of limitations of LF model, in particular, related to local angle of attack exceeding the linear lift regime and resulting error in local forces.

In Figure 14 the OASPL calculated at three observer positions using HF and LF models are presented. Although the correlations between data sets are very high, a significant difference in noise prediction is observed. The LF model gives SPL values around  $2dB$  higher than HF, even for cases for which  $C_T$  and  $C_Q$  are similar. The differences in SPL prediction remain similar throughout the whole sample. As long as this (most likely: SPL-overpredicting nature of LF model) is properly treated within the optimization framework, it does not limit the usefulness of LF model.

### 4.3 Variable-fidelity framework for propeller design optimization

The selection of candidate models to be used in the variable-fidelity optimization process can be considered as its first step. With the knowledge of models fidelity, their computational cost, limitations etc., the optimization strategy can be defined. The computational cost of models used in this work is summarized in Table 5. The values given in the time column are approximate — and may depend

Table 4 – Correlations between LF and HF results obtained for test sample.

	correlation
$C_T$	0.86
$C_Q$	0.89
$OASPL_{mic0}$	0.94
$OASPL_{mic1}$	0.88
$OASPL_{mic2}$	0.95

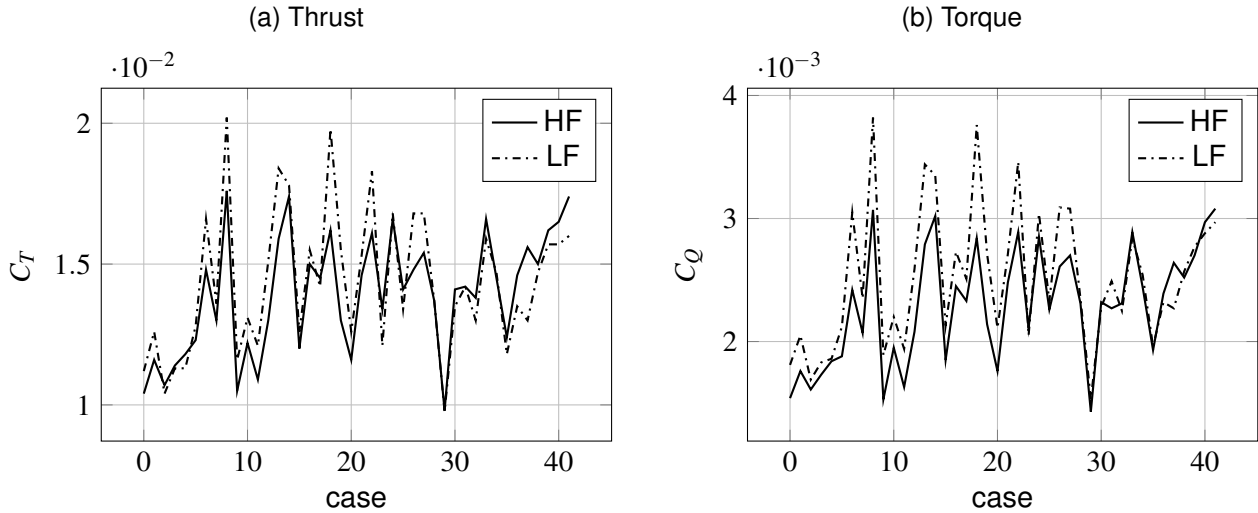


Figure 13 – Thrust and torque calculated for test sample using HF and LF models.

on different settings. HF CFD model computational cost assumes use of 20 processes. If more resources are available, this can be greatly reduced. LF aerodynamic model is computed in single process, with majority of time spent on preparation of input data. It assumes that the airfoil data table — containing data for a range Reynolds numbers — is available. The determination of such table with XFOIL takes a few minutes, once determined, the table is used for all cases. The tonal noise calculations are relatively fast for both models, while it takes around 1 minute on single process to calculate broadband noise. Further parallelization of models can be achieved for LF aerodynamics, tonal noise and broadband noise calculations. These are calculated on PC using single process.

Table 5 – Approximate computational cost (time) of evaluating low and high-fidelity models described in this study.

model	time [minutes]	hardware
HF aero	500	20 processes, cluster
LF aero	0.1	single process, PC
HF tonal noise	0.5	cluster
LF tonal noise	0.5	PC
broadband noise	1	single process, PC

The aeroacoustic analysis (i.e. involving calculation of both aerodynamics and acoustics) takes around 1.6 minutes for LF model and 501.6 minutes for HF model, which gives the HF/LF time ratio of over 300. Therefore, the LF model cost is considered to be small enough to not influence the sampling. More specifically, HF sampling should be optimized, while any reasonable number of LF samples is acceptable.

### 5. Summary

The study of different models to be used in variable-fidelity optimization was performed. High-fidelity CFD model was steady RANS  $k-\omega$  SST with periodic boundary conditions. Noise was calculated us-

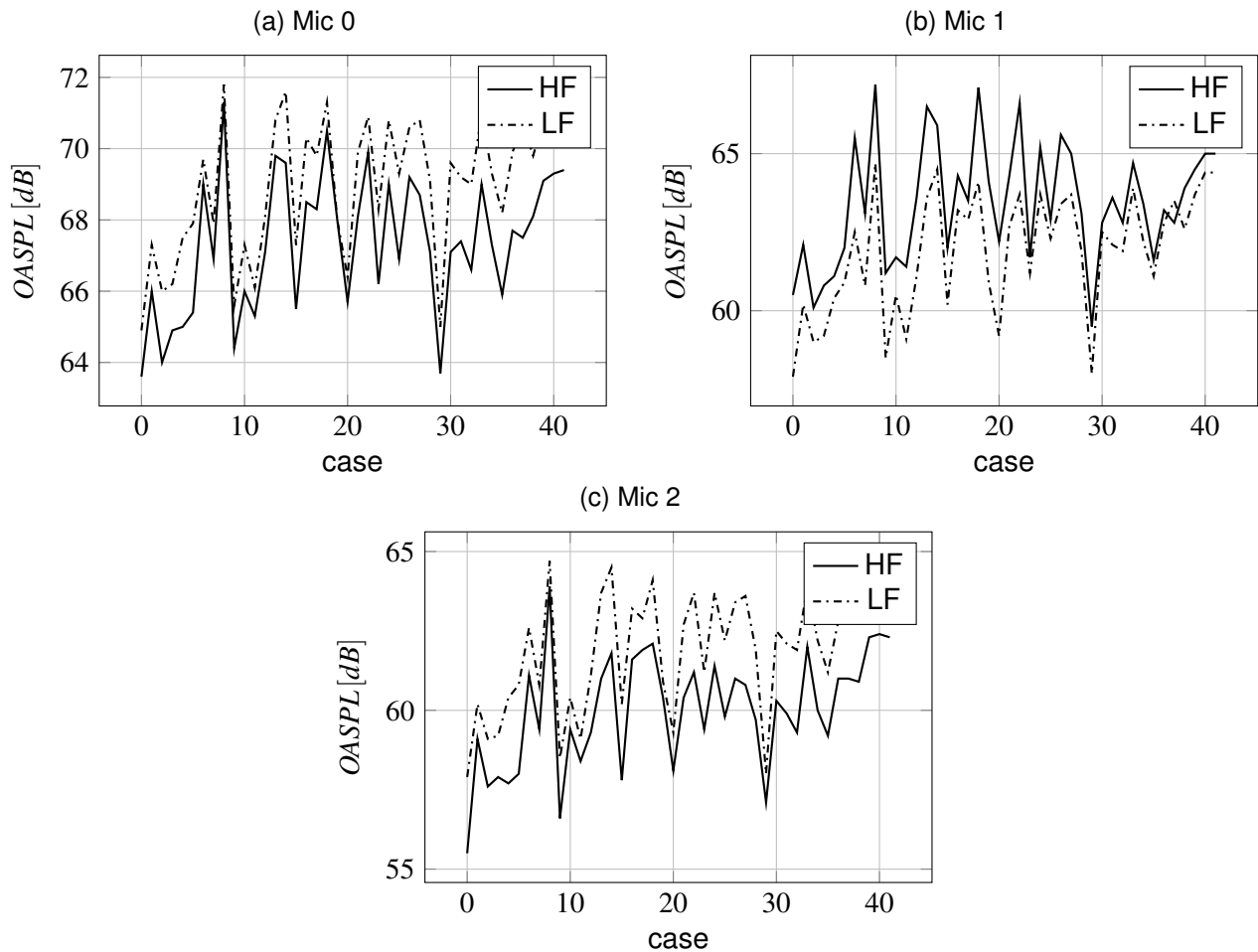


Figure 14 – Overall SPL at three microphones, in-plane, downstream and upstream of rotor calculated for test sample using HF and LF models.

ing non-permeable FWH for tonal noise component. Low-fidelity aerodynamic model was BET/vortex method code with XFOIL-based airfoil data. Based on the aerodynamic model, the noise emission was found using non-permeable FWH from pressure distribution found using XFOIL at a number of stations along the blade. The key conclusions of the work are:

- The aerodynamic low-fidelity model based on blade element/vortex method has limited accuracy in hover — scenario with relatively large effect of interactions with preceding blade tip vortex.
- Consequently, noise prediction based on the LF aerodynamic model has limited accuracy.
- The trends and correlations established for LF and HF models, basing on the representative samples, prove that the selected models are well suited for multi-fidelity optimization.
- The cost of HF model is over 300 times the cost of LF model, which focuses the sampling on minimization of the number of HF samples.

### 5.1 Future work

The following aspects will be addressed in further studies:

- Development of a mid-fidelity model, based on the resolved blade geometry and cheaper formulation. Possibilities include: one-equation turbulence model with coarser mesh and/or allowing not fully converged simulations. This model can be used in three levels-multi-fidelity optimization process, or in place of the current LF model.

- Use of high-fidelity model as input to broadband model — turbulence intensity, length scale and effective angle of attack can be extracted directly from CFD model, and extend the analysis to include the estimation of the turbulent inflow noise.
- Development of high-fidelity model based on the scale-resolving-simulation (SRS) model to allow turbulence-resolved broadband noise prediction.
- Extension of the analysis by adding varying airfoils and more elaborate tip geometry.

## 6. Contact Author Email Address

witold.klimczyk@ilot.lukasiewicz.gov.pl

## 7. Copyright Statement

The authors confirm that they, and/or their company or organization, hold copyright on all of the original material included in this paper. The authors also confirm that they have obtained permission, from the copyright holder of any third party material included in this paper, to publish it as part of their paper. The authors confirm that they give permission, or have obtained permission from the copyright holder of this paper, for the publication and distribution of this paper as part of the ICAS proceedings or as individual off-prints from the proceedings.

## References

- [1] A. I. Forrester, A. Sóbester, and A. J. Keane, “Multi-fidelity optimization via surrogate modelling,” en, *Proceedings of the Royal Society A: Mathematical, Physical and Engineering Sciences*, vol. 463, no. 2088, pp. 3251–3269, Dec. 2007. (visited on 01/28/2022).
- [2] D. R. Jones, “A taxonomy of global optimization methods based on response surfaces,” *Journal of global optimization*, vol. 21, no. 4, pp. 345–383, 2001, ISBN: 1573-2916 Publisher: Springer.
- [3] A. Kafkas, S. Kilimtzidis, A. Kotzakolios, V. Kostopoulos, and G. Lampeas, “Multi-Fidelity Optimization of a Composite Airliner Wing Subject to Structural and Aeroelastic Constraints,” en, *Aerospace*, vol. 8, no. 12, p. 398, Dec. 2021. (visited on 01/29/2022).
- [4] S. Koziel, Y. Tesfahunegn, and L. Leifsson, “Variable-fidelity CFD models and co-Kriging for expedited multi-objective aerodynamic design optimization,” en, *Engineering Computations*, vol. 33, no. 8, pp. 2320–2338, Nov. 2016. (visited on 12/28/2021).
- [5] S. Choi, J. J. Alonso, I. M. Kroo, and M. Wintzer, “Multifidelity Design Optimization of Low-Boom Supersonic Jets,” en, *Journal of Aircraft*, vol. 45, no. 1, pp. 106–118, Jan. 2008. (visited on 01/29/2022).
- [6] L. Huang, Z. Gao, and D. Zhang, “Research on multi-fidelity aerodynamic optimization methods,” en, *Chinese Journal of Aeronautics*, vol. 26, no. 2, pp. 279–286, Apr. 2013. (visited on 01/29/2022).
- [7] D. J. Toal and A. J. Keane, “Efficient multipoint aerodynamic design optimization via cokriging,” *Journal of Aircraft*, vol. 48, no. 5, pp. 1685–1695, 2011.
- [8] Z.-H. Han and S. Görtz, “Hierarchical Kriging Model for Variable-Fidelity Surrogate Modeling,” en, *AIAA Journal*, vol. 50, no. 9, pp. 1885–1896, Sep. 2012. (visited on 01/30/2022).
- [9] D. J. Toal, “Some considerations regarding the use of multi-fidelity kriging in the construction of surrogate models,” *Structural and Multidisciplinary Optimization*, vol. 51, no. 6, pp. 1223–1245, 2015.
- [10] F. Farassat, “Linear acoustic formulas for calculation of rotating blade noise,” *AIAA journal*, vol. 19, no. 9, pp. 1122–1130, 1981.
- [11] D. Casalino, E. Grande, G. Romani, D. Ragni, and F. Avallone, “Definition of a benchmark for low reynolds number propeller aeroacoustics,” *Aerospace Science and Technology*, vol. 113, p. 106707, 2021.
- [12] F. R. Menter, “Two-equation eddy-viscosity turbulence models for engineering applications,” en, *AIAA Journal*, vol. 32, no. 8, pp. 1598–1605, Aug. 1994. (visited on 01/28/2022).

- [13] K. S. Brentner and F. Farassat, "Modeling aerodynamically generated sound of helicopter rotors," *Progress in aerospace sciences*, vol. 39, no. 2-3, pp. 83–120, 2003.
- [14] J. F. Williams and D. L. Hawkings, "Sound generation by turbulence and surfaces in arbitrary motion," *Philosophical Transactions for the Royal Society of London. Series A, Mathematical and Physical Sciences*, pp. 321–342, 1969.
- [15] M. Drela, "Qprop formulation," *Massachusetts Inst. of Technology Aeronautics and Astronautics*, Cambridge, MA, 2006.
- [16] —, "Xfoil: An analysis and design system for low reynolds number airfoils," *Low Reynolds number aerodynamics*, pp. 1–12, 1989.
- [17] S. A. Rizzi, D. L. Huff, D. D. Boyd, *et al.*, "Urban Air Mobility Noise: Current Practice, Gaps, and Recommendations," NASA, Tech. Rep. NASA/TP-2020-5007433, Oct. 2020.
- [18] T. F. Brooks, D. S. Pope, and M. A. Marcolini, "Airfoil Self-Noise and Prediction," NASA Langley Research Center, Hampton, VA, Tech. Rep., 1989, p. 142.
- [19] P. Moriarty, G. Guidati, and P. Migliore, "Prediction of Turbulent Inflow and Trailing-Edge Noise for Wind Turbines," in *11th AIAA/CEAS Aeroacoustics Conference*, ser. Aeroacoustics Conferences, American Institute of Aeronautics and Astronautics, May 2005. (visited on 05/31/2022).
- [20] P. Moriarty, *NAFNoise User's Guide*, 2005.
- [21] M. D. Morris and T. J. Mitchell, "Exploratory designs for computational experiments," *Journal of statistical planning and inference*, vol. 43, no. 3, pp. 381–402, 1995.